The effect of π-stacking, h-bonding, and electrostatic interactions on the ionization energies of nucleic acid bases: adenine-adenine, thymine-thymine and adenine-thymine dimers

Ksenia B. Bravaya[a], Oleg Kostko[b], Musahid Ahmed[b], and Anna I. Krylov[a]

[a] Department of Chemistry, University of Southern California, Los Angeles, CA 90089-0482, USA

[b] Chemical Sciences Division, Lawrence Berkeley National Laboratory, Berkeley, CA 94720, USA

A combined theoretical and experimental study of the ionized dimers of thymine and adenine, TT, AA, and AT, is presented. Adiabatic and vertical ionization energies (IEs) for monomers and dimers as well as thresholds for the appearance of the protonated species are reported and analyzed. Non-covalent interactions strongly affect the observed IEs. The magnitude and the nature of the effect is different for different isomers of the dimers. The computations reveal that for TT, the largest changes in vertical IEs (0.4 eV) occur in asymmetric h-bonded and symmetric π-stacked isomers, whereas in the lowest-energy symmetric h-bonded dimer the shift in IEs is much smaller (0.1 eV). The origin of the shift and the character of the ionized states is different in asymmetric h-bonded and symmetric stacked isomers. In the former, the initial hole is localized on one of the fragments, and the shift is due to the electrostatic stabilization of the positive charge of the ionized fragment by the dipole moment of the neutral fragment. In the latter, the hole is delocalized, and the change in IE is proportional to the overlap of the fragments' MOs. The shifts in AA are much smaller due to a less efficient overlap and a smaller dipole moment. The ionization of the h-bonded dimers results in barrierless (or nearly barrierless) proton transfer, whereas the π-stacked dimers relax to structures with the hole stabilized by the delocalization or electrostatic interactions.

I. INTRODUCTION

Oxidative and radiative damage of DNA involves ionization of the individual building blocks, and the nucleotides — thymine (T), cytosine (C), adenine (A) and guanine (G) are

most likely to be ionized. Based on the gas-phase IEs, G is the easiest to ionize, however, the positive charge does not remain on G and migrates along the DNA strand as far as 200 Å[1–3]. The mechanism of the hole transfer facilitated by thermal fluctuations is not fully understood. Thermal fluctuations induce structural changes in nucleotides and in their local environment that affect so-called site energies, which can be described as IEs of the nucleotides at the specific configuration, and these dynamical changes in the local IEs drive the hole migration. Many factors may affect local IEs of the nucleotides: structural deformations of the nucleotide itself, presence of the backbone, interaction with the solvent, hydrogen bonding, π-stacking, and electrostatics. Thus, understanding how different type of interactions affect the IEs is the first step toward a mechanistic understanding of the ionization-induced dynamics in DNA. Another crucial mechanistic question is how does the hole migration occur. Once the site energies of the neighboring bases match, does the hole simply hop from a higher to a lower energy site, or is there a transient hole delocalization over two (or more) bases involved?

Similar mechanistic questions about the role of non-covalent interactions in charge transport through molecular wires arise in the context of molecular electronics[4–10].

A fundamental understading of radiation-induced processes in individual bases and their clusters are also important for astrobiology and prebiotic chemistry[11].

While IEs of the nucleic acid bases (NAB) in the gas phase have been characterized both experimentally[12–18] and computationally[19–22], much less is known quantitatively about the effects of different interactions on IEs in a realistic environment. Similar to electronically excited states[23–28], the ionized states are adversely affected by base stacking, base pairing via hydrogen bonding, electrostatic interactions, and solvent effects. The latter have been reported to lower IEs of anionic nucleotides and to reduce the gap between them and phosphate IE suggesting that nucleotide ionization becomes more favorable in water[29, 30]. Likewise, microsolvation of the nucleobases decreases their IEs by about 0.1 eV per water molecule[16, 18]. Base pairing and other hydrogen bonding interactions also reduce IEs and oxidation potentials, as discussed in a computational study of Crespo-Hernández *et al.*[31].

Recently, the effects of h-bonding and π-stacking on the IEs of two isomers of the uracil dimer were characterized by high-level electronic structure calculations[32]. Earlier studies of the effects of π-stacking on IEs of nucleobases include Hartree-Fock and DFT estimates

using Koopmans theorem[33–37], MP2 (Møller-Plesset perturbation theory) and CASPT2 (perturbatively-corrected complete active space self-consistent field) calculations[19, 21, 38].

In this work, we present the combined experimental and theoretical investigation of IEs of AA, TT, and AT dimers in the gas phase. The focus of this work is on the effects of non-covalent interactions, i.e., hydrogen bonding, π-stacking, and electrostatic interactions, on the IEs of the individual nucleobases. We also analyze the changes in electronic structure (i.e., hole localization and proton transfer) induced by these interactions.

The structure of the paper is as follows. The next section presents experimental and theoretical details. Section III discusses equilibrium structures and binding energies of the representative neutral dimers, and vertical IEs (VIEs). For selected dimers, we also report optimized geometries of the cations and adiabatic IEs (AIEs). The theoretical results are compared with the experimentally measured spectra in Section III F. Our final remarks are given in Section IV.

II. EXPERIMENTAL AND COMPUTATIONAL METHODS

A. Experimental details

The experiments were performed on a molecular beam apparatus coupled to a 3 meter VUV monochromator on the Chemical Dynamics Beamline at the Advanced Light Source (ALS). The clusters of the NAB are prepared by thermal desorption (T=495 K) of individual bases (A,T), as well as simultaneous desorption of two bases (A and T), and cooled in a supersonic beam. In the latter experiments, both homo- and hetero clusters are produced. The thermal vaporization source has been described recently in a publication detailing the microsolvation of DNA bases[18]. In the current experiments, the backing pressure of Ar expanded through a 100 μm diameter nozzle was 35 kPa. The clusters are ionized by tunable synchrotron radiation in the 7.4-11.5 eV region, and the ions are detected by a time-of-flight mass spectrometer. For each mass, the yield of the ions is measured as a function of photon energy, which produces photoionization efficiency (PIE) spectra. The typical step size for the PIE scans is 50 meV, and a dwell time of 10 s at a repetition rate of 10 kHz. The differentiation of the PIE curves following the method used by Berkowitz in interpreting photoionization of methanol[39] produces a spectrum similar to a photoelectron spectrum

from which information about vibrational progressions and other electronic states can be extracted. The differentiation is performed numerically after taking a five points nearest-neighbor average to reduce the effects of noise in the PIE. The accuracy of reported onset energies in the PIE spectra is 0.05 eV.

For protonated species (BH^+), which arise at M+1 mass, where M is a mass of neutral monomer, corrections have to be made to account for the natural abundance of isotopes constituting M. This amounted to 7.47% and 6.46% of the M signal for A and T, respectively, which was subtracted from the M+1 signal to provide the true BH^+ signal. The error in determination of the appearance energies of AH^+ and TH^+ species is $\pm$0.1 eV. The lower accuracy and the small negative signal (see Supporting Information) in this case comes from the overlap of the M and M+1 bands in the mass spectra, in case of which contribution of the isotope-corrected M signal to M+1 band by can be overestimated.

B. Theoretical methods and computational details

Accurate description of equilibrium geometry of nucleobases dimers requires methods capable of treating attractive dispersion forces originating from the correlated motion of electrons. Density functional theory (DFT) often used for geometry optimizations of extended molecules fails to reproduce these interactions[40]. The wave function based MP2 method underestimates intermolecular distances[41], and the results are very sensitive to basis set superposition error (BSSE). An inexpensive solution is offered by empirically corrected DFT in which the standard functionals are augmented by R^{-6} terms[42]. Geometries of the neutral dimers were optimized with the B3LYP-D dispersion-corrected functional with the s_6 scaling factor of 1.05 as suggested by Grimme *et al.* [43] and the 6-31+G(d,p) basis set. The basis set effects as well as the performance of B3LYP-D functional were tested for the AT stacked dimer from the S22 set. We found that increasing the basis set from 6-31+G(d,p) to 6-311++G(2df,2pd) results in a slight increase (0.004 Å) of the interfragment distance, and that the B3LYP-D/6-31+G(d,p) value differs from the BSSE-corrected RI-MP2/TZVPP result [44] by 0.076 Å.

For geometry optimizations of the cationic open-shell species we employed long-range and dispersion-corrected ωB97X-D functional [45] with the same basis set. This functional includes long-range Hartree-Fock exchange to mitigate the notorious self-interaction error

that becomes particularly important in ionized dimers. This functional when used with 6-311++G(3df,3pd) basis set was shown to describe geometries and binding energies of the weakly bound complexes with the mean absolute errors of 0.064 Å and 0.22 kcal/mol, respectively [45]. Based on the relatively small basis set dependence of the B3LYP-D equilibrium geometries of the neutral AT dimer, we expect similar errors for the ωB97X-D/6-31+G(d,p) structures.

The standard SG-1 grid was used for the DFT-D geometry optimization. Tight convergence criteria of 1.2×10^{-4}, 1×10^{-7} and 3×10^{-5} for atomic displacement, energy change and gradient, respectively, were used due to the shallow potential energy surface of weakly bound neutral stacked dimers.

Binding energies of the neutral and cationic dimers were estimated by ωB97X-D/6-311++G(2df,2pd) single point calculations with a fine EML(75,302) grid consisting of 75 points in the Lebedev [46] radial grid and 302 points in the Euler-Maclaurin [47] angular grid. To verify the structures the Hessians were computed with the ωB97X-D/6-31+G(d,p) method and the EML(75,302) for dimer isomers used for ionization energies computations. The ωB97X-D/6-31+G(d,p) optimized geometries were used for binding energies estimations and Hessian computations. Thermodynamic analysis was performed within rigid rotor — harmonic oscillator — ideal gas approximation (RR-HO-IG) for the standard conditions (T=298.18 K, p=1 atm). The relative populations of different isomers were estimated at standard conditions, as well as at T=495 K (experimental desorption temperature).

Vertical and adiabatic IEs are computed using equation-of-motion coupled-cluster method with single and double substitutions (EOM-CCSD) [48–50] for ionization potentials (EOM-IP-CCSD) [51–55], which is capable of describing multiple closely lying electronic states in an accurate, robust and efficient computational scheme. The method is free from artifactual symmetry breaking and spin-contamination that often plague the description of open-shell species. The EOM-IP-CCSD methodology has been successfully applied to characterize spectroscopic signatures of hole delocalization in ionized non-covalent dimers such as benzene dimers [55, 56], h-bonded and π-stacked uracil dimers [32], and water clusters [57, 58].

VIEs of the monomers and dimers were computed with the EOM-IP-CCSD method and the cc-pVTZ and 6-311+G(d,p) basis sets, respectively. Core electrons were frozen in all calculations. In addition, EOM-IP-CCSD/6-311+G(d,p) calculations also employed

resolution of identity (RI) approximation with the auxiliary aug-cc-pVTZ basis set. The errors due to RI are below 1×10^{-4} eV for the thymine monomer. In dimers calculations, the virtual orbital subspace for the EOM-IP-CCSD calculations was truncated by using frozen natural orbitals (FNO) approximation [59] with the natural population threshold of 99.5 %. This approach was tested on thymine and the errors were found be less than 0.1 eV for the six lowest ionized states with respect to the full virtual space results. Even better performance (errors below 0.05 eV) was observed for guanine[59]. The errors of the FNO approximation with the same occupation threshold were found to be even smaller for the uracil dimer: the mean error for ten lowest IEs is 0.03 eV for EOM-IP-CCSD/6-311+G(d,p)[59].

The lowest AIEs were obtained as the difference between the EOM-IP-CCSD energy of the first ionized state at the cation geometry and the CCSD energy of the reference state at the geometry of the neutral.

An energy additivity scheme was used to estimate the EOM-IP-CCSD/cc-pVTZ IEs of the dimers assuming that the basis set effects in the monomers and dimers are similar [32]. The approximated EOM-IP-CCSD/cc-pVTZ (large basis, LB) VIEs of the dimers were computed from EOM-IP-CCSD/6-311+G(d,p) (small basis, SB) VIEs using the following expression[32]:

$$IE^{LB}_{dimer,i} = IE^{SB}_{dimer,i} + (IE^{LB}_{monomer,j} - IE^{SB}_{monomer,j}) \quad (1)$$

where i and j are the number of dimer ionized state and corresponding monomer ionized state. Energy additivity scheme was used for each ionized state of the dimer separately by applying basis set correction for the corresponding state of the monomer. This can be done only for the states that are of a Koopmans-like character and correlate well with the states of the monomers. When the ionized states acquire mixed character manifesting itself in multi-configurational wave functions (e.g., as in the AT stacked dimer), the correction become more difficult to apply. Adiabatic IEs were extrapolated using the correction for the lowest vertical IEs.

Natural charges for the first ionized state of the dimers were computed with NBO package [60] for IP-CISD/6-31+G(d,p) electron density. In the IP-CISD method [61] ionized states are described as linear combination of singly ionized and ionized and excited (1h and 2h1p, respectively) determinants derived from the closed-shell Hartree-Fock reference. This approach is an N^5 approximation to EOM-IP-CCSD in which the HF determinant is employed to descroibe the reference state instead of the CCSD wave function.

Optimized geometries, relevant total energies, and harmonic frequencies are given in Supporting Information. All calculations were performed using the *Q-CHEM* electronic structure program[62].

III. RESULTS AND DISCUSSION

A. Binding energies and structures of the neutral dimers

The NAB dimers form numerous isomers[63–65], and their populations in the molecular beam may be non-thermal. For example, higher energy isomers were observed in several experimental studies using laser desorption[65, 66].

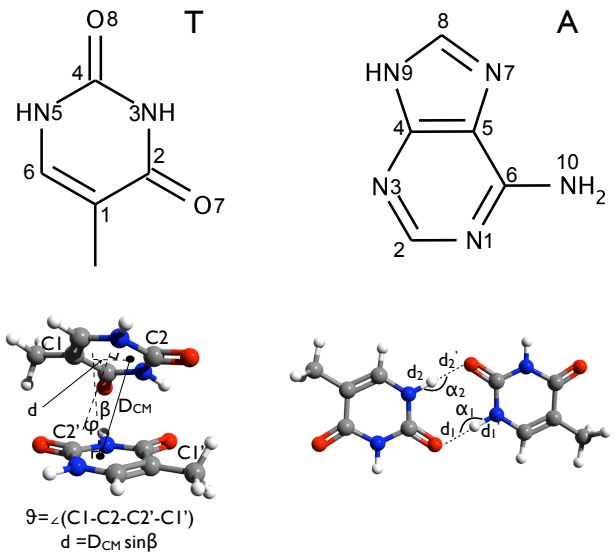

FIG. 1: Top: Chemical structures of adenine and thymine with atomic numeration used in the text. Bottom: Definitions of the main parameters characterizing geometries of stacked and h-bonded NAB dimers. For the stacked dimers, these parameters are: distance between the centers of mass (COM) of the fragments (D_{CM}), tilt angle between the planes of the bases (φ), the relative twist of the fragments (θ), and the horizontal displacement of the COM (d). For the h-bonded dimers, the most important structural parameters are the distances between the atoms participating in h-bonding (d and d') and the corresponding angles (α).

There are three principally different types of relative fragment arrangement in the NAB dimers, i.e., h-bonded, stacked and t-shaped structures. The t-shaped dimers are predicted

to be higher in energy than the h-bonded manifold[67]. Moreover, one can expect that intermolecular interactions have the smallest effect on the IEs in the case of t-shaped dimers relative to the h-bonded and stacked dimers. Therefore, we considered only the h-bonded and stacked isomers.

Fig. 1 shows the typical structures of the stacked and h-bonded dimers, and defines important structural parameters characterizing relative orientation of the fragments. The values of these parameters for several isomers are summarized in Tables I and II, and several representative stacked and h-bonded structures are shown in Figs. 2 and 3, respectively.

Binding energies of the several lowest-energy h-bonded and π-stacked AA, TT, and AT isomers are presented in Table III. For the cations, dissociation energies for $B^{+\cdot}$ + B and several BH^+ + $(B–H)^{\cdot}$ channels are given. Binding energies of selected π-stacked and h-bonded isomers are shown in Figs. 2 and 3. In agreement with numerous previous studies (see, for example, Refs[67–69] and references therein), the most stable dimer is a symmetric (C_{2h}) h-bonded one with two monomers being equivalent (TT-HB1 and AA-HB1). In TT, there are several non-symmetric h-bonded dimers with non-equivalent fragments (4-5 kcal/mol higher than the lowest-energy one), which are stabilized by electrostatic dipole-dipole interactions (note longer h-bond lengths in TT-HB2 and TT-HB3 relative to TT-HB1). The lowest-energy stacked dimer appears only 8-10 kcal/mol above the lowest h-bonded one, and is followed by four (TT) or five (AA) more isomers within 2.5 kcal/mol of each other (see Fig. 2).

Close inspection of Fig. 2 and Table I reveals important structural differences between stacked TT and AA isomers, which have important implications on change of IEs due to the stacking interactions. In TT, the lowest-energy π-stacked isomers have good overlap of the polar NH and CO bonds. The five lowest isomers lying within 2.5 kcal/mol range have favorable overlap of several polar bonds. Thus, TT π-stacked structures are dominated by electrostatic interactions. In AA, the situation is different: in the six lowest isomers (which are within 2 kcal/mol), the fragments are less aligned. Some of the isomers are stabilized by the inter-fragment interactions similar to h-bonding, e.g., five of them have the NH2 hydrogens of the one fragment pointing towards nitrogen atoms of the other fragment. However, the structures reveal that these bonds are relatively long and, consequently, are weaker than regular hydrogen bonds. Thus, they do not appear to be the dominant factor, for example, one of the isomers (AA-ST5) has no h-bonds at all and seems to be stabilized

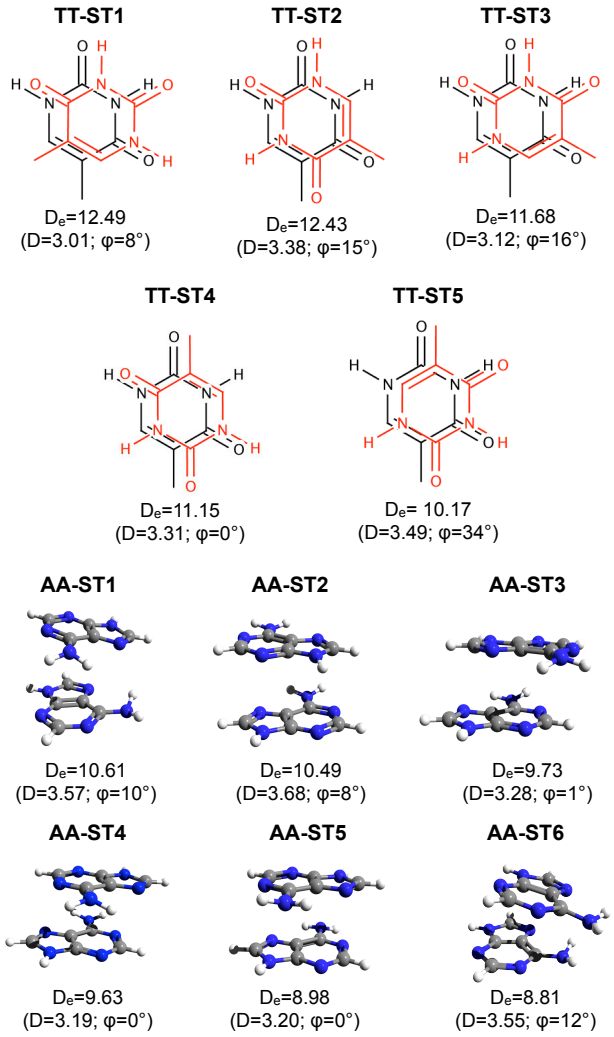

FIG. 2: Structures of the TT (top) and AA (bottom) stacked dimers and their binding energies (D_e, kcal/mol) and selected structural parameters (see Fig. 1) computed at the B3LYP-D/6-31+G(d,p) level of theory.

mostly by dipole-dipole interactions and dispersion. Both the TT and AA isomers are floppy: the six lowest frequencies corresponding to relative motions of the fragments vary from 20 to 100 cm^{-1} and are remarkably similar in AA and TT. The upshot of these structural differences is that the fragments in TT structures are aligned better and are more equivalent (in 3 isomers both fragments are identical by symmetry), whereas in AA the fragments have different local environments. Both factors contribute to better orbital overlap and larger hole delocalization in TT, which is confirmed by the shapes of MOs and atomic charges, as

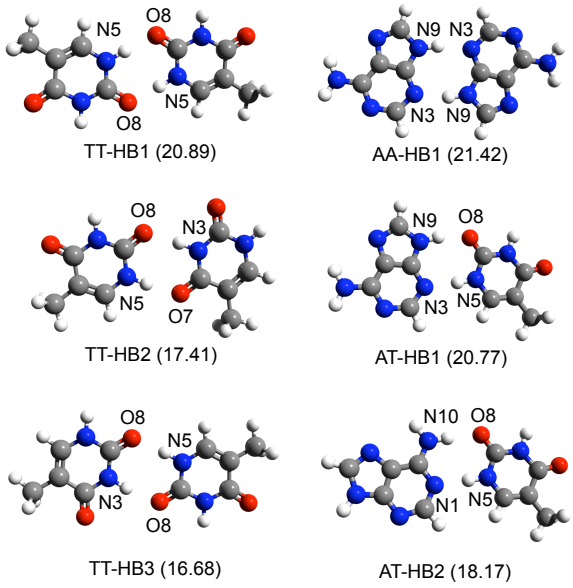

FIG. 3: Structures of selected h-bonded dimers of T and A bases. B3LYP-D/6-31+G(d,p) dissociation energies (kcal/mol) are presented in parentheses.

discussed below.

Binding energies (D_e and D_0), which are presented in Table III, reveal that ZPE has a small effect on binding energies of the neutrals reducing them by 1-2 kcal/mol in both h-bonded and stacked dimers.

For the AT dimers, we considered two h-bonded dimers (AT-HB1 and AT-HB2) and one stacked (AT-ST1). AT-HB1 is the lowest energy dimer and the AT-HB2 h-bonded isomer is the one observed by IR-UV spectroscopy [70] in a molecular beam experiment, which is 2.9 kcal/mol higher in energy (Table III). The authors [70] reported two structures that could not be distinguished in that experiment. We considered the lowest energy structure of these two.

B. Free energy calculations

In an earlier work on uracil dimer, Hobza and coworkers discussed possible entropy effects, which may favor π-stacked relative to h-bonded isomers [71]. ΔS is negative for dimerization, however, the π-stacked dimers have higher entropy because of floppier structures, and,

TABLE I: Optimized intermolecular structural parameters (see Fig. 1) for the neutral and ionized stacked NAB dimers[a].

Isomer	Symmetry	State	D_{CM}, Å	φ (tilt)	θ (twist)	d, Å
TT-ST1	C_2	neutral	3.01	8°	37°	0.28
TT-ST2	C_1	neutral	3.38	15°	65°	0.74
TT-ST3	C_1	neutral	3.12	16°	63°	0.15
TT-ST4	C_i	neutral	3.31	0°	180°	1.04
TT-ST5	C_2	neutral	3.49	34°	180°	1.14
TT-ST1	C_1	cation	3.04	0°	41°	0.23
TT-ST3	C_1	cation	3.52	16°	69°	1.37
AA-ST1	C_1	neutral	3.57	10 °	90°	1.93
AA-ST2	C_1	neutral	3.68	8°	171°	1.73
AA-ST3	C_1	neutral	3.28	1°	2°	1.13
AA-ST4	C_i	neutral	3.19	0°	180°	0.67
AA-ST5	C_1	neutral	3.20	0°	180°	0.17
AA-ST6	C_1	neutral	3.55	12°	20°	1.66
AA-ST1	C_1	cation	3.25	2°	121°	1.03
AT-ST1	C_1	neutral	3.10	7°	28°	0.26
AT-ST2	C_1	neutral	3.07	6°	82°	0.12
AT-ST3	C_1	neutral	3.38	9°	37°	1.57

[a]Geometries of the neutrals and the cations were optimized with B3LYP-D/6-31+G(d,p) and ωB97X-D/6-31+G(d,p), respectively.

therefore, ΔS for their formation is less negative relative to h-bonded ones. A later paper from Hobza and coworkers[67], where they performed full-dimensional (rather than reduced 6D, as in the uracil study) NVE calculations, does not show any π-stacked population in non-methylated pairs except for AA, where they report 3% of the stacked isomer. In this paper, the authors emphasize that entropy is not important, in contradiction to their uracil work. In another MD simulation study from the same authors [68], significant (10, 10 and 25 % for AA, AT and TT, respectively) populations of the higher-energy stacked isomers were reported. Thus, first-principle predictions of the populations of different structures are

TABLE II: Optimized intermolecular structural parameters (see Fig. 1) for the neutral and ionized h-bonded NAB dimers.[a]

Isomer	Symm	State	d_1/d_1', Å	α_1	d_2/d_2', Å	α_2
TT-HB1	C_{2h}	neutral	1.767/1.031 (O8···H/H−N5)	178	1.031/1.767 (N5−H/H···O8)	178
TT-HB1 (TS)[b,c]	C_{2h}	cation	1.704/1.037 (O8···H/H−N5)	174	1.037/1.704 (N5−H/H···O8)	174
TT-HB1 (HT)[d]	C_s	cation	1.027/1.608 (O8−H/H···N5)	174	1.033/1.745 (N5−H/H···O8)	174
TT-HB2	C_s	neutral	1.764/1.030 (O7···H/H−N5)	175	1.034/1.814 (N3−H/H···O8)	173
TT-HB2 (HT)[d]	C_s	cation	1.022/1.629 (O7−H/H···N5)	172	1.037/1.756 (N3−H/H···O8)	173
TT-HB3	C_s	neutral	1.779/1.029 (O8···H/H−N5)	175	1.033/1.825 (N3−H/H···O8)	172
TT-HB3 (HT)[d]	C_s	cation	1.039/1.567 (O8−H/H···N5))	173	1.034/1.787 (N3−H/H···O8)	172
AA-HB1	C_{2h}	neutral	1.851/1.037 (N3···H/H−N9)	167	1.037/1.851 (N9−H/H···N3)	167
AA-HB1[b]	C_{2h}	cation	1.854/1.037 (N3···H/H−N9)	166	1.037/1.854 (N9−H/H···N3)	166
AA-HB1 (HT)[d]	C_s	cation	1.045/1.793 (N3−H/H···N9)	164	1.034/1.888 (N9−H/H···N3)	167
AT-HB1	C_1	neutral	1.840/1.038 (N3(A)···H/H−N5(T))	178	1.028/1.801 (N9(A)−H/H···O8(T))	164
AT-HB1[b]	C_1	cation	2.197/1.016 (N3(A)···H/H−N5(T))	170	1.083/1.485 (N9(A)−H/H···O8(T))	176
AT-HB1 (HT)[d]	C_s	cation	1.039/1.866 (N3(A)−H/H···N5(T))	176	1.019/1.904 (N9(A)−H/H···O8(T))	149
AT-HB2	C_1	neutral	1.846/1.039 (N1(A)···H/H−N5(T))	178	1.023/1.845 (N10(A)−H/H···O8(T))	176
AT-HB2	C_1	cation	2.122/1.018 (N1(A)···H/H−N5(T))	167	1.081/1.505 (N10(A)−H/H···O8(T))	176
AT-HB2 (HT)	C_s	cation	1.036/1.913 (N1(A)−H/H···N5(T))	175	1.022/1.827 (N10(A)−H/H···O8(T))	168

[a]Structural parameters for geometries of the neutrals and the cations optimized with ωB97X-D/6-31+G(d,p). [b] Not h-transferred. [c] TS: transition state. [d] HT: h-transferred.

TABLE III: ωB97X-D//ωB97X-D/6-31+G(d,p) binding energies (kcal/mol) of several lowest-energy h-bonded and stacked TT, AA and AT dimers.

isomer	state	D_e	D_e	ZPE	ΔZPE[a]	D_0 [b]
		6-31+G(d,p)	6-311++G(2df,2pd)			
TT-HB1	neutral	19.28	19.33	147.012	1.056	18.22
	cation (HT)	30.27[c], 39.62[d]	30.78[c], 39.75[d]	145.632	0.640[c], -1.343[d]	30.14[c], 39.15[d]
TT-HB2	neutral	15.56	16.04	147.104	1.148	14.89
	cation (HT)	32.66[c], 36.28[d]	32.00[c], 36.21[d]	145.757	0.765[c], 0.895[d]	31.24[c], 35.49[d]
TT-HB3	neutral	14.88	15.38	146.992	1.036	14.34
	cation	28.09	28.46	144.635	-0.357	28.82
	cation (HT)	28.80[c], 37.44[d]	29.30[c], 37.26[d]	145.262	0.270, 0.739	29.03[c], 37.03[d]
TT-ST1	neutral	11.49	11.59	146.531	0.575	10.92
	cation	19.80	19.33	146.052	1.060	18.27
TT-ST3	neutral	10.22	10.46	146.872	0.916	9.55
	cation	20.07	19.44	145.867	0.875	18.47
AA-HB1	neutral	20.78	19.85	143.715	1.167	18.68
	cation (HT)	34.54[c], 35.81[d]	34.06[c], 34.71[d]	144.069	1.306[c],1. 165[d]	32.75[c],33.40[d]
AA-ST1	neutral	10.66	10.55	144.123	1.575	8.97
	cation	21.92	21.36	143.738	0.975	20.38
AT-HB1	neutral	19.80	19.22	145.410	1.158	18.06
	cation	21.31	21.14	144.546	0.079	21.06
	cation (HT)	30.28[c], 28.83[d]	39.87[c] , 28.20 [d]	144.861	0.394[c],0.886[d]	29.48[c],27.31[d]
AT-HB2	neutral	16.89	16.55	145.644	1.392	15.16
	cation	19.77	19.42	144.789	0.322	19.45
	cation (HT)	31.32[c], 28.31[d]	30.90[c], 27.89[d]	145.180	0.713[c], 1.204[d]	29.70[c], 26.69[d]
AT-ST1*	neutral	12.39	12.38	—	—	—

* The AT ST1 structure is a transition state at the wB97X-D/6-31+G(d,p) level of theory and a true minimum with no imagine frequencies optimized with B3LYP-D/6-31+G(d,p). The two geometries are very close. [a] Difference between the ZPEs of the dimer and the monomers. ZPE(A)=71.274 kcal/mol, ZPE(A^+)=71.489 kcal/mol, ZPE(AH^+N1)=80.098 kcal/mol, ZPE(A–H)$^{\cdot}$=62.807 kcal/mol, ZPE(T)=72.978 kcal/mol, ZPE(T^+)=72.014 kcal/mol, ZPE(TH^+O8)=80.624 kcal/mol, ZPE(TH^+O8_1)=80.645 kcal/mol, ZPE(TH^+O7)=80.984 kcal/mol and ZPE((T–H)$^{\cdot}$)=63.878 kcal/mol. ZPE values for the monomers were computed with the ωB97X-D/6-31+G(d,p)//ωB97X-D/6-31+G(d,p) method and the EML(75,302) grid. [b] Binding energies corrected by ZPE (D_0). [c] Dissociation to B^+ and B. [d] Direct dissociation to BH^+ and (B–H).

not yet reliable, even under well-defined statistical ensemble conditions.

Furthermore, it is not entirely clear how populations in the beam prepared by thermal or laser desorption should be modeled, and whether the evaporation can be considered as an equilibrium process. Supersonic cooling is another non-equilibrium step involved in our experiment [72]. Thus, it is not surprising that there is extensive experimental evidence that the populations in these beams are non-thermal (see Ref. [72] and references therein). For example, the only AT dimer isomer registered by IR-UV spectroscopy in a molecular beam with gas species formed by thermal evaporation is not the lowest energy one but one, which is higher by 2.8 kcal/mol [70]. In the case of adenine dimers, the lowest energy symmetric structure was not observed experimentally in the gas phase, while the next two structures were identified [73]. Thus, the results of our estimates of the thermal populations presented below should not be taken as quantitative predictions of the populations in the experiment.

Free energy computations within the RR-HO-IG approximation point to dominant population of h-bonded dimers in molecular beam at 298 and 495K, the latter corresponds to the experimental thermal evaporation conditions (see Table IV). The entropy factor ($T\Delta S$) is different for the stacked and h-bonded dimers of favoring formation of the stacked dimers. For AA, the entropy contributions for the stacked and h-bonded systems are nearly the same (Table IV).

Thus, although the entropy contribution slightly favors π-stacked structures over h-bonded, the overall effect in the differences of the Gibbs free energy is small, i.e., about 1-2 kcal/mol at 298 K for TT, and even less (0.02-0.06 kcal/mol) for AA. More appropriate treatment of the floppy modes beyond the RR-HO-IG approximation may enhance the effect.

To conclude, while it is difficult to estimate populations of different isomers in the beam, there is sufficient experimental and theoretical support for the presence of multiple isomers including, perhaps, even higher-energy stacked ones.

C. Character of the ionized states and VIEs

Fig. 4 compares raw and differentiated PIE curves for the monomers and the dimers from a pure thymine or adenine molecular beam. Also shown are appearance energy curves for protonated adenine and thymine. The protonated species are formed via dissociative

TABLE IV: Total H (kcal/mol) and S (cal/mol·K) in the RR-HO-IG approximation and ΔH_r^0 (kcal/mol), ΔS_r^0 (cal/mol·K) and ΔG_r^0(kcal/mol) for the dimer formation from the monomers (T=298.18 K, p=1 atm.) and relative populations of the isomers at 298 and 495 K.

	H	S	ΔH_r^0 [a]	ΔS_r^0	ΔG_r^0	$p_i^{T=298.18K}$ [b]	$p_i^{T=495K}$ [b]
TT-HB1	157.851	127.915	-18.433	-43.575	-5.44	1	1
TT-HB2	158.383	136.183	-14.611	-37.307	-3.49	$3.7 \cdot 10^{-2}$	$4.8 \cdot 10^{-1}$
TT-HB3	158.336	137.006	-13.998	-36.484	-3.12	$2.0 \cdot 10^{-2}$	$3.9 \cdot 10^{-1}$
TT-ST1	157.614	132.060	-10.930	-41.430	1.42	$9.3 \cdot 10^{-6}$	$1.4 \cdot 10^{-3}$
TT-ST3	158.324	135.506	-9.090	-37.984	2.24	$2.3 \cdot 10^{-6}$	$1.2 \cdot 10^{-3}$
AA-HB1	154.415	129.976	-18.461	-40.194	-6.48	1	1
AA-ST1	154.698	129.895	-8.878	-40.275	3.13	$9.1 \cdot 10^{-8}$	$5.6 \cdot 10^{-5}$
AT-HB1	156.457	135.155	-17.753	-36.675	-6.82	1	1
AT-HB2	156.505	134.965	-15.035	-36.865	-4.04	$9.2 \cdot 10^{-3}$	$5.7 \cdot 10^{-2}$

[a] Using D_e computed at the ωB97X-D/6-311++G(2df,2pd)/ωB97X-D/6-31+G(d,p) level of theory; H(A)=76.513 kcal/mol, S(A)=85.085 cal/mol·K, H(T)=78.477 kcal/mol, S(T)=86.745 cal/mol·K.

[b] The ratio of the populations of the particular isomer relative to the most stable one.

photoionization of the respective dimers or larger clusters. The TT spectrum features a prominent red shift (0.35 eV) in the onset (AIE), as well as noticeable changes in relative intensities of different bands. AA exhibits a strikingly different pattern: the changes in the shape of the first band are smaller and the onset is red-shifted by only 0.10 eV (although, it is difficult to determine the onset due to the low intensity of the first band). Overall, Fig. 4 demonstrates the strong effect of dimerization on the IEs.

The changes in IEs due to stacking or h-bonding interactions are determined by orbitals' overlap and delocalization [33–35], as well as electrostatic perturbations by the local environment. These changes, as well as the fate of the ionized states, can be rationalized within the dimer molecular orbital — linear combination of fragment molecular orbitals (DMO-LCFMO) framework [56, 57]. Below we discuss VIEs and the character of ionized states of several representative isomers of TT, AA, and AT dimers, and explain the changes due to clustering interactions.

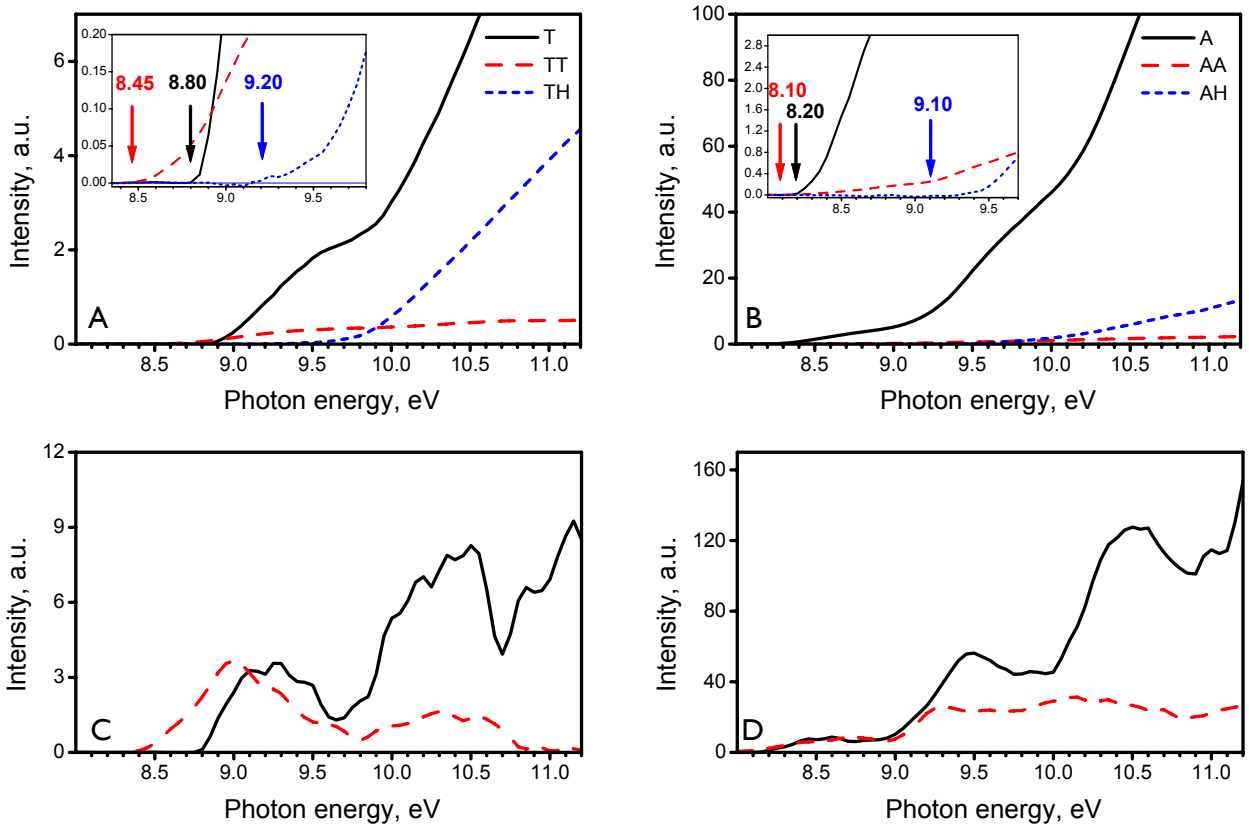

FIG. 4: Raw (A,B) and differentiated (C,D) PIE curves for monomers and dimers of thymine (A,C) and adenine (B,D).

TABLE V: Adiabatic and vertical IEs (eV) of the TT, AA, and AT dimers.

	EOM-IP-CCSD/6-311+G(d,p)									
State	TT-HB1	TT-HB2	TT-HB3	TT-ST1	TT-ST3	AA-HB1	AA-ST1	AT-HB1	AT-HB2	AT-ST1
1^{st} AIE	8.23	8.03	8.15	8.41	8.34	7.48	7.57	7.57	7.39	—
1	8.88	8.66	8.68	8.71	8.92	8.23	8.16	8.36	8.30	8.26
2	9.00	9.04	9.10	9.23	9.06	8.26	8.21	8.81	8.64	8.71
3	10.03	9.77	9.78	10.02	9.91	9.36	9.21	9.57	9.59	9.61
4	10.09	10.14	9.89	10.07	10.02	9.43	9.25	9.60	9.79	9.83
5	10.48	10.16	10.17	10.28	10.20	9.49	9.30	9.94	9.81	9.91
6	10.53	10.29	10.28	10.39	10.43	9.49	9.48	10.31	10.17	9.99
	Extrapolated EOM-IP-CCSD/cc-pVTZ (see text)									
1^{st} AIE	8.30	8.12	8.23	8.48	8.41	7.50	7.59	7.60	7.42	—
1	8.95	8.73	8.76	8.78	8.99	8.25	8.18	8.39	8.33	8.28
2	9.07	9.11	9.17	9.30	9.13	8.28	8.23	8.88	8.71	8.89
3	10.13	9.88	9.89	10.12	10.02	9.39	9.25	9.59	9.62	9.32
4	10.19	10.25	9.99	10.17	10.13	9.46	9.29	9.64	9.81	9.51
5	10.59	10.27	10.28	10.39	10.31	9.52	9.31	10.04	9.91	9.97
6	10.64	10.40	10.39	10.50	10.54	9.51	9.50	10.40	10.26	10.07

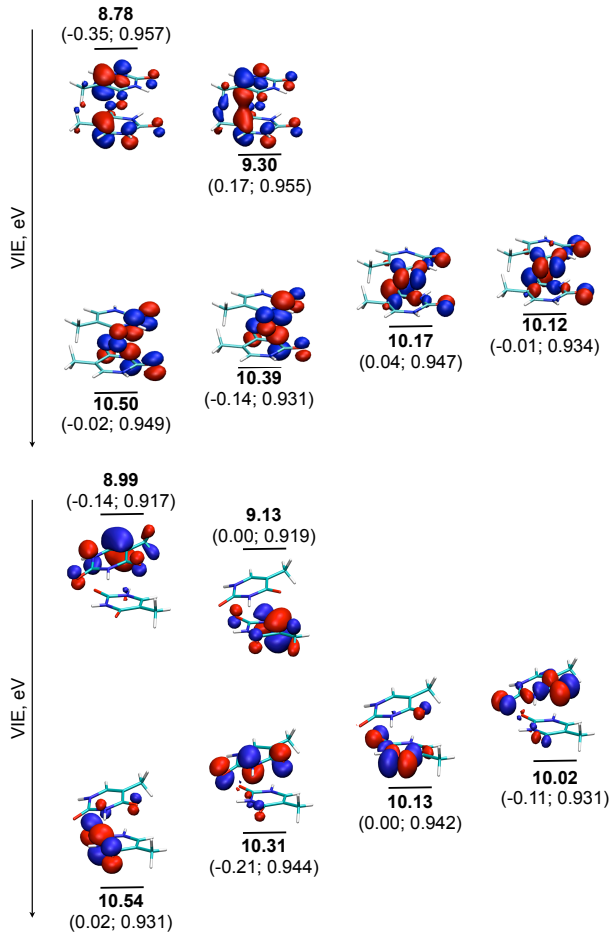

FIG. 5: The MOs and respective VIEs (eV, EOM-IP-CCSD/6-311+G(d,p) extrapolated to cc-pVTZ) for the two stacked TT dimers, TT-ST1 (top) and TT-ST2 (bottom). Energy difference (eV) between the dimer IE and corresponding IE of the monomer and leading EOM amplitudes for shown orbitals are given in parenthesis.

Table V summarizes vertical and adiabatic IEs of TT, AA, and AT dimers. Figures 5-7 show the MOs and the corresponding VIEs (as well as the changes in IEs relative to the monomer values) for the (i) two π-stacked dimers, TT-ST1 and TT-ST3 (Fig. 5); (ii) the lowest-energy symmetric h-bonded dimer, TT-HB1 (Fig. 6); and (iii) two non-symmetric h-bonded dimers, TT-HB2 and TT-HB3 (Fig. 7). These energies are computed by EOM-IP-CCSD/6-311+G(d,p) and extrapolated to EOM-IP-CCSD/cc-pVTZ by using energy additivity scheme, Eq. (1).

In the symmetric π-stacked isomer (TT-ST1, D_0=10.9 kcal/mol), the fragments are equivalent, and the dimer MOs are in-phase and out-of-phase linear combinations with equal

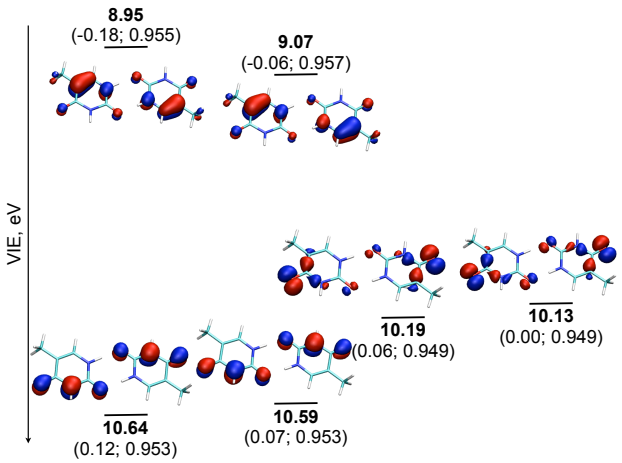

FIG. 6: The MOs and respective VIEs (eV, EOM-IP-CCSD/6-311+G(d,p) extrapolated to cc-pVTZ) for the lowest-energy h-bonded TT dimer, TT-HB1. Energy difference (eV) between the dimer IE and corresponding IE of the monomer and leading EOM amplitudes for shown orbitals are given in parenthesis.

weights. The structure, in which the π_{CC} bond of one fragment is on top of the π_{CC} bond of another fragment, results in large overlap of fragments HOMOs. At the equilibrium geometry of the neutral dimer, the ionization from the higher (anti-bonding) orbital is 0.35 eV lower than that of the monomer, whereas the ionization from the bonding orbital is 0.17 eV higher. The fate of these two ionized states is very different. Ionization from the anti-bonding orbital increases formal bond order between the fragments, and the fragments move closer to maximize the overlap and increase the bonding interactions (discussed in Section III E). Ionization from the lower orbital, has bonding character, results in a purely repulsive inter-fragment potential leading to dissociation. Higher states of the cation, which are derived from lower lying MOs, exhibit a similar pattern, with the respective splitting depending strongly on the overlap (for example, IEs corresponding to the ionization from in-plane oxygen lone pairs are much closer to the respective monomer values[32]).

The situation is rather different in a slightly higher TT isomer (TT-ST3, D_0=9.6 kcal/mol), which has lower symmetry. Because the fragments are no longer equivalent, the dimer MOs are less delocalized and the energy splitting between them is smaller. The corresponding VIEs are much closer to the monomer values, e.g., the lowest VIE is only 0.14 eV lower than that of the monomer. The initial hole is localized, and one may expect that both states relax to a bound ionized dimer.

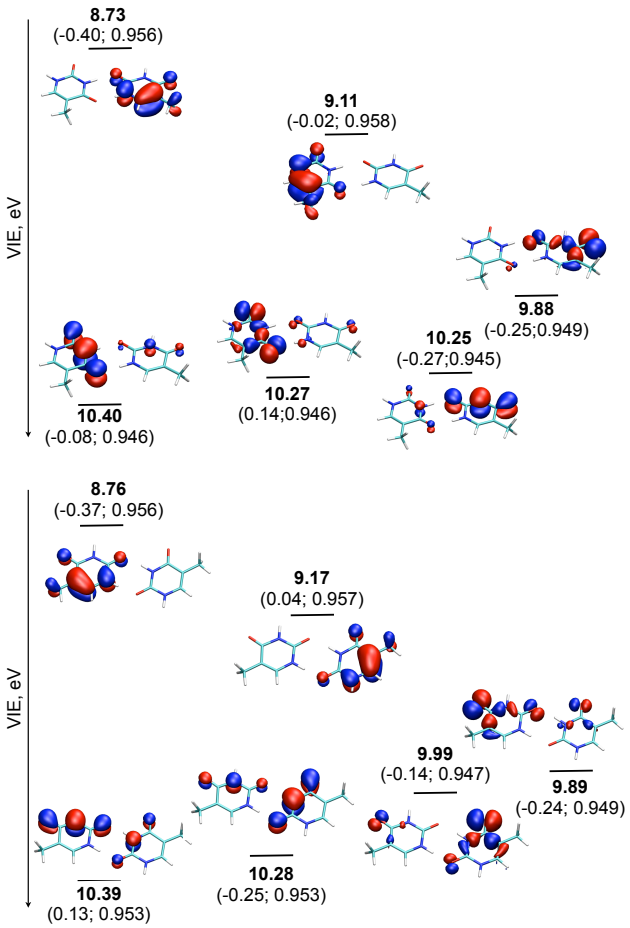

FIG. 7: The MOs and respective VIEs (eV, EOM-IP-CCSD/6-311+G(d,p) extrapolated to cc-pVTZ) for two non-symmetric h-bonded dimers, TT-HB2 (top) and TT-HB3 (bottom). Energy difference (eV) between the dimer IE and corresponding IE of the monomer and leading EOM amplitudes for shown orbitals are given in parenthesis.

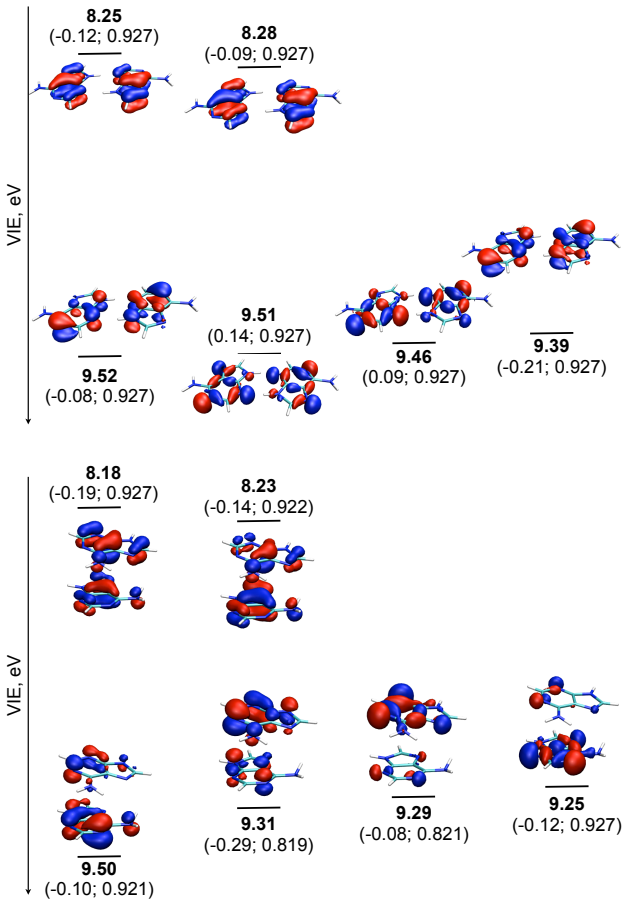

FIG. 8: The MOs and respective VIEs (eV, EOM-IP-CCSD/6-311+G(d,p) extrapolated to cc-pVTZ) for the H-bonded (top) and stacked (bottom) AA dimers. Energy difference (eV) between the dimer IE and corresponding IE of the monomer and leading EOM amplitudes for shown orbitals are given in parenthesis.

The lowest energy h-bonded dimer (D_0=18.2 kcal/mol) presents a different pattern. Because the monomers' HOMOs are of π type, their overlap in the h-bonded structure is small. Consequently, the changes in IE are smaller. Interestingly, both in-phase and out-of-phase orbitals are destabilized, the respective VIEs are 0.18 and 0.06 eV lower than the monomer value. Due to the symmetry constraints, the initial hole is delocalized over the two monomers, however, the corresponding optimized cation structure is not a minimum but a saddle point with a negative frequency along the asymmetric h-transfer mode. Thus, ionization of the h-bonded TT results in barrierless h-transfer forming an asymmetric $(TH)^+(T–H)^{\cdot}$ dimer in which the charge is localized on the TH fragment, and the unpaired

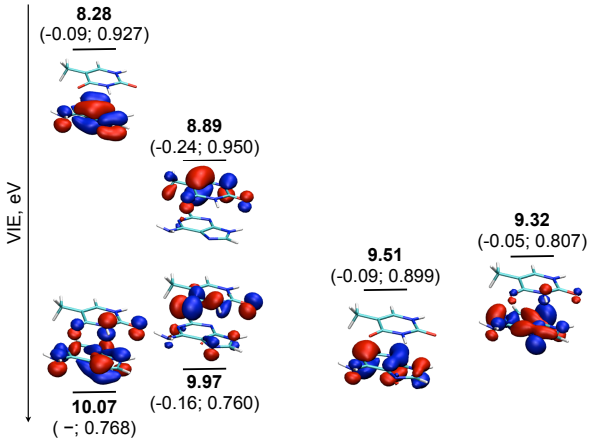

FIG. 9: The MOs and respective VIEs (eV, EOM-IP-CCSD/6-311+G(d,p) extrapolated to cc-pVTZ) for the stacked AT dimer. Energy difference (eV) between the dimer IE and corresponding IE of the monomer and leading EOM amplitudeis for shown orbital are given in parenthesis.

electron — on the $(T–H)^{\cdot}$ moiety (see Sec. III E).

Quite surprisingly, two higher energy h-bonded isomers (TT-HB2, D_0=14.9 and TT-HB3, D_0=14.3 kcal/mol) feature yet another pattern: while orbitals are localized on the monomers, the changes in VIEs are large (0.37-0.40 eV for the 1st ionized state) and comparable to those in the symmetric π-stacked isomer. In these non-symmetric isomers the fragments are not equivalent, and the changes in VIEs are due to the electrostatic field exerted by the fragments (the dipole moment of the neutral T is 4.11 D), as explained below.

The inspection of the EOM amplitudes (given in Figures 5- 7) shows that the ionized states in the TT dimers are of a Koopmans-like character, e.g., the leading amplitudes corresponding to ionization of the respective Hartree-Fock orbitals are above 0.9. The electron correlation, however, is very important for accurate energetics and affects the IEs by more than 1 eV.

VIEs for the representative AA dimers are presented in Table V and in Fig. 8. The h-bonded isomer (AA-HB1) shows trends similar to TT-HB1, i.e., both in-phase and out-of-phase orbitals are destabilized by 0.09 and 0.12 eV, respectively. The stacked AA dimer behaves differently: the changes in VIEs are smaller than those for TT-ST1 dimer due to the less efficient orbital overlap. Both HOMO and HOMO-1 IEs are reduced by 0.19 and 0.14 eV, respectively. Moreover, some of the higher states show more localized character.

Interestingly, two of the dimer states show more substantial configuration interaction,

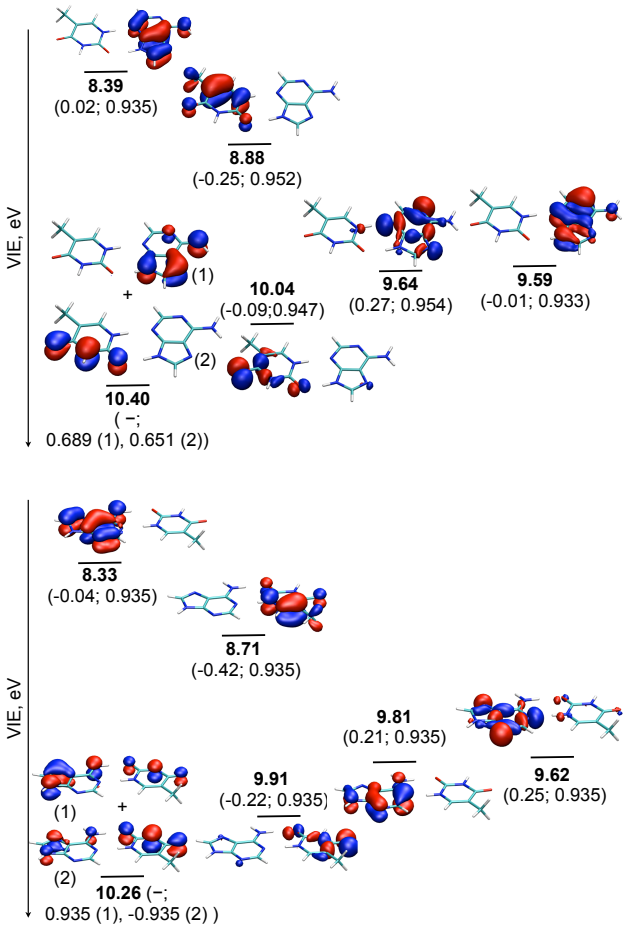

FIG. 10: The MOs and respective VIEs (eV, EOM-IP-CCSD/6-311+G(d,p) extrapolated to cc-pVTZ) for the h-bonded AT-HB1 (top) and AT-HB2 (bottom) dimers. Energy difference (eV) between the dimer IE and corresponding IE of the monomer and leading EOM amplitudes for shown orbitals are given in parenthesis.

i.e., the leading EOM amplitudes drop to about 0.8.

Table V and Fig. 9 and 10 present the VIEs for the representative AT dimers. The fragments are non-equivalent owing to their different chemical nature, and, consequently, the MOs are more localized. The lowest VIE for the AT-ST1 dimer (Fig. 9) corresponds to the ionization of A (the NBO charge on the A fragment is 0.99), and is 0.09 eV lower than that of the monomer. The next ionized state is localized on T, and its VIE is 0.24 eV lower than that of bare T, but 0.52 eV above the VIE of A. The h-bonded isomers show similar trend — the lowest ionization corresponds to the A, and the next one — to the T moiety (Fig. 10). An interesting pattern observed in these two isomers is that IEs of the A

fragment are affected much less than those of T, at least for the low-lying states.

Some of the states in AT dimers are profoundly non-Koopmans, as evidenced by the EOM amplitudes. In these states, Hartree-Fock orbitals do not provide an accurate description of the ionized states, and correlated Dyson orbitals should be employed to characterize the hole[22, 74].

D. The effect of non-covalent interactions on VIEs: A semi-quantitative analysis

To explain the origin of the shifts of the VIES of the NA bases dimers in comparison to the monomers as well as splitting between dimer ionized states, and to interpret these quantities in terms of interfragment orbital overlap and electrostatic interactions two simple models were used. The DMO-LCFMO approach [56, 57] can be extended to provide a more quantitative analysis of the changes in the IEs in dimers with equivalent fragments. As discussed in Ref. [56], a 3-electrons-in-2-orbitals problem can be mapped into a 1-electron-in-2-orbitals one. The dimer states are obtained by diagonalizing a 2x2 Hamiltonian matrix of the two interacting monomer states, which yields the following value for the energy splitting, ΔE_{12}, between the states:

$$\Delta E_{12} = \frac{H_{11}S_{12} - H_{12}}{1 - S_{12}^2} \tag{2}$$

where H_{11} is the energy level of the non-interacting fragments, H_{12} is the respective coupling matrix element, and S_{12} is the overlap between the fragments' MOs. To extract these parameters from the electronic structure calculations, we employ a locally-projected HF procedure [75] in which the SCF solution for the dimer is obtained in the basis of the MOs that are strictly localized on the fragments. We use the matrix elements of the Fock operator to parametrize Eq. (2), i.e., the F_{12} matrix element is used as H_{12}, and the diagonal elements are replaced by the orbital energies. These calculations were performed with 6-311+G(d,p) basis set.

This scheme was used to estimate splitting energies for the three lowest pairs of ionized states of the symmetric h-bonded AA (AA-HB1) and TT (TT-HB1) dimers, as well as symmetric stacked TT dimer (TT-ST1). To increase the number of states in the analysis, we also included the two h-bonded and one stacked symmetric cytosine dimers (see Supporting Information). Overall, 18 pairs of ionized states were included in the analysis.

Fig. 11 (upper panel) compares the splittings computed by EOM-IP-CCSD/6-

311+G(d,p) with the values estimated by Eq. (2). The two sets of ΔE_{12} show good correlation (R^2=0.96), except for the three points marked by the arrows that correspond to the ionized states of a non-Koopmans character (i.e., having large EOM amplitudes for more than one orbital). Since Eq. (2) is derived based on a one-electron model, these states were excluded from the fitting procedure. Fig. 11 (lower panel) also shows that the splittings correlate well (R^2=0.91) with orbital overlap S_{12}. Thus, the magnitude of splittings in the symmetric dimers can be well reproduced by a simple one-electron model parametrized by the locally-projected HF calculations. However, the analysis becomes more complicated in the case of dimers comprised of two non-equivalent fragments, where more elaborate parametrization is required [10, 76].

The origin of large shifts in IEs in non-symmetric h-bonded dimers (TT-HB2 and TT-HB3) is different. We analyzed this effect by computing the energy of electrostatic interactions between the atomic NBO charges on the ionized fragment with the dipole moment of the other fragment using the following expression:

$$E = \sum_i E(r_i, \theta) = \frac{q_i |D|}{r_i^2} \left[cos\theta + \frac{1}{8} \left(\frac{|D|}{r_i} \right)^2 \left(5cos^3\theta - 3cos\theta \right) + \ldots \right] \qquad (3)$$

where r_i is the distance between atom i of fragment 1 and COM of fragment 2, q_i is a NBO charge on the ith atom, $|D|$ is the norm of the dipole moment vector, and θ is the angle between dipole moment vector and $\boldsymbol{r}_i$. The center of the dipole moment is positioned in the COM of fragment 2. Only the first two terms of the expansion were taken into account. The partial charges and the dipole moment were computed for the isolated ionized and neutral fragments at their geometries in the dimer. This model is only valid for the non-symmetric dimers with the localized ionized states. The computed energies for the eight states of the two asymmetric h-bonded TT dimers and two states of cytosine dimer (see Supporting Information) correlate well with the observed shifts in VIE, as shown in Fig. 12.

E. Equilibrium structures of the ionized dimers and their adiabatic IEs

Changes in geometries of symmetric stacked isomers upon ionization (see Tables I and II) are consistent with DMO-LCFMO predictions — the fragments adjust to maximize the orbital overlap. Because the orbitals are not completely delocalized, the relaxation does not

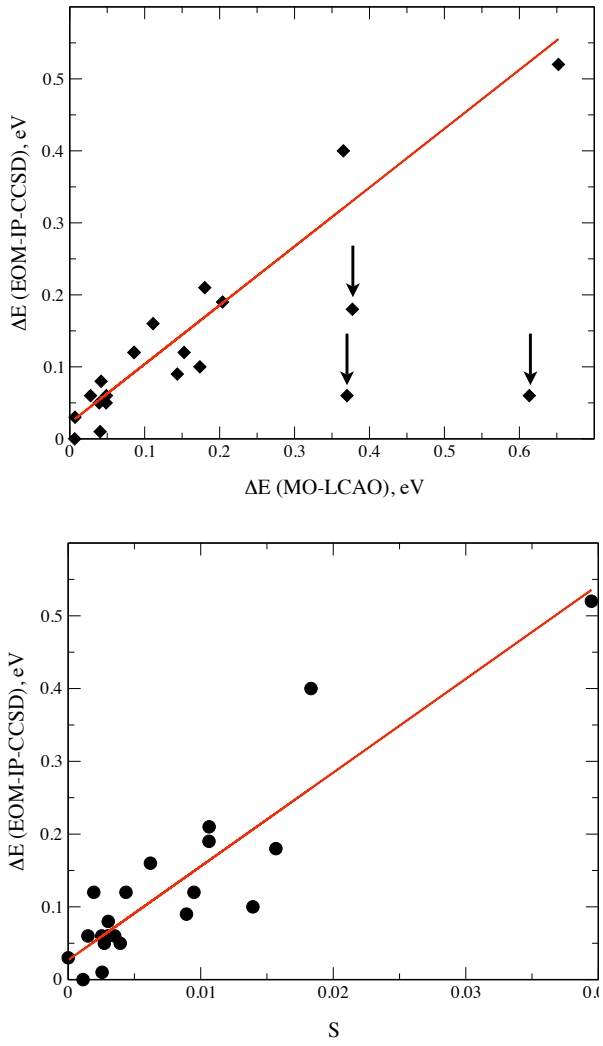

FIG. 11: Energy splittings between the ionized states computed by EOM-IP-CCSD/6-311+G(d,p) versus the DMO-LCFMO values (upper panel) and the orbital overlap (lower panel).

necessarily reduce the D_{CM}. For example, in TT-ST1 the distance between COM actually increases, however, the fragments also become more parallel (tilt angle changes from 8° to 0°), and the horizontal displacement decreases. TT-ST1 cation relaxes to the C_1 symmetry structure. The TT-ST1 structure optimized with C_2 symmetry constrains lies slightly higher in energy (0.4 kcal/mol) and is characterized by two imaginary frequencies, corresponding to the tilt motion and relative shift of the two thymine rings. These changes reduce the distance between two double CC bonds (hosting most of the HOMO density). The optimized structure of TT-ST3 isomer (that has a localized hole) shows 0.4 Å increase in D_{CM} and also a large increase in horizontal displacement (1.22 Å). This structure is stabilized by the

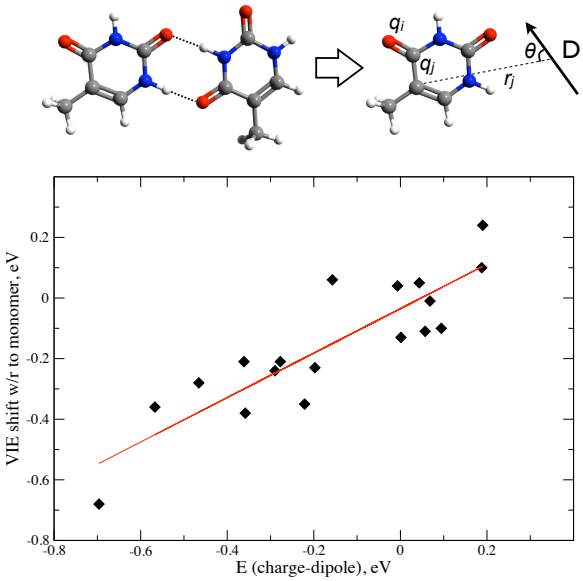

FIG. 12: VIE shifts versus charge-dipole interaction energy for eight states of the asymmetric TT-HB2 and TT-HB3 dimers and two states of the asymmetric CC dimer, see text.

CO group of the "neutral" fragment pointing towards the positive charge localized on the C=C bond of the "ionized" fragment.

The partial covalent bond formed between the fragments due to ionization results in an increase in binding energies relative to the neutrals. For example, the D_0 of TT-ST1 increases from 10.92 kcal/mol (neutral) to 18.27 kcal/mol (cation), see Table III. The lowest AIE of the TT-ST1 is 8.48 eV. The optimization of the non-symmetric stacked dimer, TT-ST3, converges to an asymmetric structure in which the charge is localized on one fragment. The NBO charges for the optimized TT-ST3 cation are 0.85 and 0.15 for the two T fragments. The positive charge on one of the fragments is stabilized by the oxygen lone pairs of the second fragment pointing towards it. The D_0 for this dimer cation is 18.47 kcal/mol, which means that this isomer is slightly below the symmetric isomer with the delocalized hole. The respective adiabatic IE is 8.41 eV.

Energetically, the relaxation in the stacked dimers is larger relative to the monomers, i.e., the VIE-AIE difference in T is 0.23 eV [77], whereas in TT-ST1 and TT-ST3 it is 0.3 and 0.58 eV, respectively. The relaxation in A is 0.25 eV, to be compared with 0.49 in AA-ST1.

Ionization of h-bonded dimers is followed by a barrierless or nearly barrierless interfragment proton transfer for most of the considered systems. Different h-bonding patterns are

likely to lead to different dissociation products. The energy diagram for the neutrals, cations and dissociation products for several dissociation channels is shown in Fig. 13.

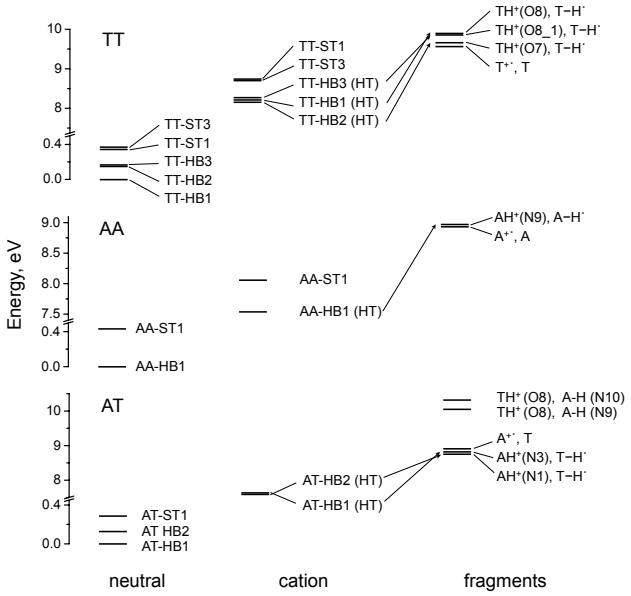

FIG. 13: Relative energies of the ionized dimers and the dissociation products with respect to the lowest energy neutral dimer for each system (TT, AA and AT). Energies are computed with ωB97X-D/6-311++G(2df,2dp)//ωB97X-D/6-31+G(d,p) and include ZPEs. The arrows indicate the channels for direct dissociation of the cationic h-transferred h-boned dimers.

The ionization of symmetric h-bonded TT (TT-HB1) results in barrierless h-transfer forming an asymmetric $(TH)^+(T–H)^{\cdot}$ dimer in which the charge is localized on the TH fragment (the NBO charge for the TH^+ moiety is 0.86). The relaxation relative to the neutral's geometry is 0.65 eV (Table V). The optimized symmetric structure, which is a saddle point with one imaginary frequency, is 0.11 eV below the vertical geometry (ωB97X-D/6-311++G(2df,2pd)//ωB97X-D/6-31+G(d,p), not shown). The adiabatic IE is rather low and equals 8.30 eV. The dissociation energy of this isomer is 1.3 eV (30.1 kcal/mol) to T and $T^{+\cdot}$, whereas dissociation energy producing TH^+(O8) and $(T–H)^{\cdot}$ is 1.7 eV (Fig. 13).

The TT-HB2 also undergoes barrierless proton transfer resulting in 0.61 eV relaxation (Table V). The respective AIE is 8.12 eV, and dissociation energies to T and $T^{+\cdot}$ and TH^+(O7) and $(T–H)^{\cdot}$ are 31.2 and 35.5 kcal/mol. The true minimum on the cation potential energy surface for TT-HB3 was located for the structure without proton transfer. However, one of the hydrogen bond is already very short in this structure (1.392 Å) and, hence,

one can expect a low barrier and fast inter-fragment proton transfer in this case as well. The structure with proton transferred from one base to another for the TT-HB3 lies below this minimum by only 1 kcal/mol. The overall relaxation of the cation from vertical to the h-transferred structure is 0.53 eV (Table V). Dissociation energies to T and $T^{+\cdot}$ and TH^{+}(O8_1) and $(T–H)^{\cdot}$ are 29.0 and 37.0 for the TT-HB3 dimer.

The lowest stacked AA isomer converges to a structure that has smaller D_{CM} and φ, which increases the orbital overlap with an AIE of 7.59 eV. AA-HB1 converges to a symmetric structure with all frequencies being real, however, this minimum is very shallow and may not be able to support a single vibrational state, e.g., an unrelaxed scan along h-transfer mode (that has an unphysically large frequency of 5,812 cm^{-1}) shows a barrier of only 2 kcal/mol. The proton transfer for the adenine dimer cation has recently been characterized by both theory and experiment [78, 79]. Although the transition state for this process was successfully localized, the inclusion of ZPE makes it process barrierless [78]. The reported energy of the proton-transferred structure relative to the vertically ionized state calculated with B3LYP/6-31+G** is -4.5 kcal/mol, which differs from our values computed with more reliable methods, i.e., ωB97X-D/6-311++G(2df,2pd) and EOM-IP-CCSD/6-311+G(d,p) yielding VIE-AIE energy difference of -19 kcal/mol and -17 kcal/mol, respectively. The agreement between these two estimates points to problematic behavior of a B3LYP in the case of open-shell species.

To summarize, the h-bonded TT and AA dimers show barrierless (or almost barrierless) proton transfer forming asymmetric [e.g., $(BH)^{+}(B–H)^{\cdot}$] structures accompanied by large energy relaxation (about 0.6 eV). These results are in agreement with previous studies suggesting increased acidity of NAB upon ionization[36, 80–85], and demonstrate that h-transfer in the ionized states is even more efficient than in the electronically excited states, where the reduced barriers have also been reported[86, 87]. It has been suggested that coupling of the proton transfer to the hole hopping process slows down the charge mobility in DNA double strand by separation of the charge and unpaired electron[81].

The AT-HB1 dimer presents an interesting case. The hole is initially localized on the adenine base and one can expect proton transfer from A to T due to the increased acidity of adenine upon ionization. Indeed, relaxation of the cation leads to a structure with a very short hydrogen bond (1.485 vs 1.801 Å for neutral) in which adenine is a proton donor. The length of the second hydrogen bond is increased from 1.840 to 2.197 Å upon ionization. The

proton transfer reaction from adenine to thymine for the AT Watson-Crick base pair has been previously studied using B3LYP/6-31G(d,p) approach [85]. The reported transition state and product energies relative to the cation minimum structure without proton transfer were 1.64 kcal/mol and 1.22 kcal/mol, respectively. However, according to our results, the structure resulting from hydrogen transfer from thymine to adenine lies much lower in energy (0.79 eV below the vertically ionized state, see Table V). The barrier for the proton transfer reaction from T to A can be significantly higher than in the case of A to T proton transfer due to the longer h-bond. AT-HB2 shows very similar trends, see Tables II and III. Geometry optimization of cationic AT-ST dimer results in hydrogen-bonded structure. This can be a result of shallow potential energy surface of the dimer cation with respect to the change of the tilt angle or artificial result of DFT-D applied to the case the molecule with two competing type of interactions: stabilization caused by orbital overlap (partial covalent character of the dimer cation) and stabilization of the cation through strong hydrogen bonding.

F. Experimental PIE curves and theoretical IEs

Fig. 14 shows differentiated PIE spectra for AA, TT for the case of pure beam and differentiated PIE of AT dimer for the mixed beam of A and T, as well as computed VIEs and the lowest AIEs for several isomers. Also indicated are threshold energies for the dissociation of the dimers to the protonated and ionized monomers. The onset of the curve corresponds to the lowest AIE, whereas the maxima can be interpreted as VIEs. One important feature of the differentiated PIE curve is that we cannot exclude contributions from fragments of higher clusters, which are likely to be produced via ionization to repulsive states, especially at higher energies. This has been shown to occur in the case of thymine and adenine by Stolow and coworkers [27]. However, due to much smaller population of larger clusters, these contributions should not be large. Examination of a mass spectrum at 10 eV reveals that under our experimental conditions, trimer contributions are around 1% to the total signal, while approximately 30% of the signal correspond to the dimer and protonated monomer, and 69% of the signal arises from the monomer

Fragmentation of the dimer giving rise to $B^{+\cdot} + B$ contributes to the monomer signal. An examination of the first band of thymine monomer in Fig. 4C shows a broad structured peak extending from 8.7 to 9.6 eV. The signal in this region could also arise from fragmentation

TABLE VI: Energy thresholds (eV) for the appearance of BH^+ and $B^{+\cdot}$ formed by the dissociation of ionized dimers computed with ωB97X-D/6-311++G(2df,2pd)//ωB97X-D/6-31+G(d,p) and including ZPE.

Species	Channel				
	TT-HB1	AT-HB1	AT-HB2		
TH^+(O8)	9.91	10.03	10.18[a]		
	TT-HB3				
TH^+(O8_1)	9.71				
	TT-HB2				
TH^+(O7)	9.54				
	TT-ST3	TT-ST1	TT-HB3	TT-HB2	TT-HB1
$T^{+\cdot}$	9.17	9.22	9.38	9.41	9.54
	AT-HB1	AA-HB1			
AH^+	8.82	8.97			
	AT-HB2				
AH^+(N1)	8.63				
	AA-ST1	AT-ST1	AT-HB1 2	AT-HB1	AA-HB1
$A^{+\cdot}$	8.51	8.61*	8.78	8.91	8.94

[a] - without ZPE correction

of the dimer, however it's difficult to separate the two contributions in our derived PIE. Our calculations for thymine show (Table VI) that this channel opens up around 9.2 to 9.5 eV (depending on the isomer) suggesting that this is indeed occurring.

Furthermore, the PIE spectra of the dimer will exclude the contributions from the dissociative states, e.g., higher state of the symmetric dimers corresponding to the ionization from the bonding orbitals. Similar difficulties arise in other types of experiments involving intermediate states, see, for example, the discussion of the electron-ion coincidence spectra in Ref. [27].

As follows from Fig. 14 and Table V, the AIEs of both TT-ST1 and TT-ST3 are very close to the experimental onset (8.45 eV). AIEs for TT-HB1, TT-HB2 and TT-HB3 dimers fall into the lower energy region. However, due to significant geometrical relaxation in the

h-bonded isomers, the FCFs are expected to be small, so it is not clear if these isomers can be seen at the onset. The sharp rise of the experimental curve suggests more favorable FCFs, as in, for example, stacked TT dimers.

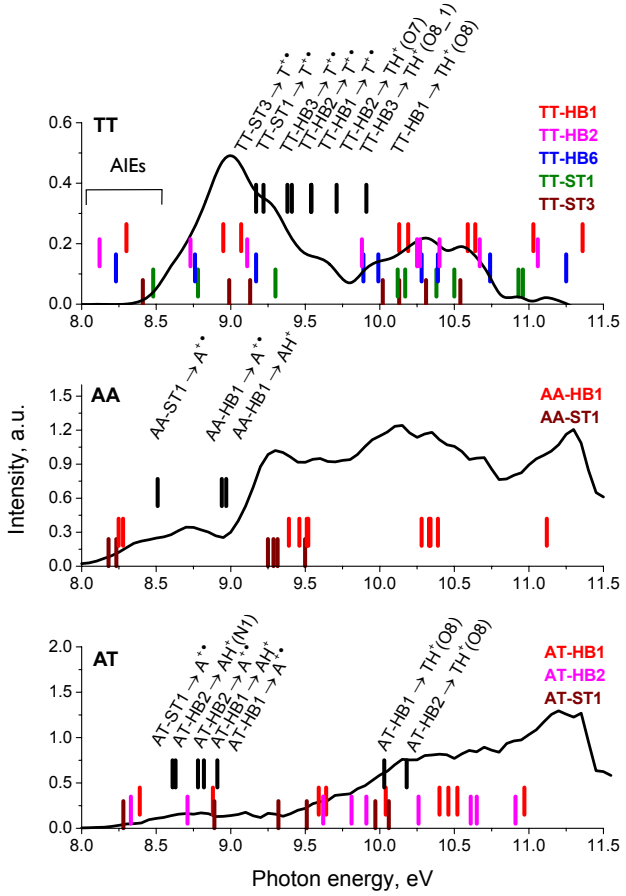

FIG. 14: Differentiated PIE curves and calculated vertical and adiabatic IEs for the selected isomers. The thresholds for the h-bonded dimers dissociation to $B^{+\cdot}$ and B as well as BH^+ and $(B–H)^{\cdot}$ are indicated by black bars. Positions of ionized states of different isomers are differentiated by color and height according to the order given in the plots legend.

As follows from the calculations, the first band can contain contributions from the states derived from HOMO and HOMO-1 ionization of T, whereas the second band can contain four more ionized states. A large red shift in vertical position is consistent with the computed values of the h-bonded isomer, whereas the lowest VIE of TT-ST1 and h-bonded TT-HB3 appear to coincide with a lower energy shoulder. Since every second line of the symmetric dimers will not appear in the dimer PIE curves (because of their dissociative nature), the large red shift is not accompanied by a broadening of the lines.

The second band presents clear evidence of at least two types of isomers: the lowest-energy h-bonded isomer explains lower and higher energy features, whereas the band maximum corresponds to the ionization derived from either one or two π-stacked isomers, or higher-energy asymmetric h-bonded TT-HB2 and TT-HB3.

The change in the relative intensities of the two bands can be explained by the fact that the cation states giving rise to the second band are energetically above the dissociation threshold (for the lowest electronic states), and are, therefore, predissociative. The appearance thresholds for the protonated species are also consistent with the computed values, as discussed below.

The AA curve has a different shape: it contains a small first band extending from 8.1 to 9.1 eV, followed by three very broad bands. Dimerization affects the two lowest ionized states of AA less than in case of TT, which can be explained by more efficient orbital overlap in the latter due to the better aligned fragments (in π-stacked isomers) and more localized monomers MOs. The dipole moment of A is also smaller, i.e., 2.61 D in comparison to 4.11 D in T (RI-MP2/cc-pVTZ), which results in smaller shifts in asymmetric h-bonded structures. The computed VIEs of AA show the changes from the monomer values of 0.12 and 0.19 eV for the lowest ionized state of h-bonded and stacked dimers, respectively, and of 0.09-0.21 eV and 0.08-0.29 eV for the upper states (Fig. 8). The AIE value for proton-transferred AA-HB1 is 7.50 eV, which is 0.60 eV below the onset of the PIE curve, 8.10 eV, whereas the symmetric h-bonded structure corresponds to the AIE of 8.15 eV. The AIE for AA-ST1 is 7.59 eV. Large geometric relaxation and poor FCFs (which are rather small even in the monomer) may be responsible for the low signal at the onset.

Differentiated PIE spectrum of the AT dimer consists of one weak band extending from 8.0 to 9.2 eV with the onset of 8.05 eV and the maximum at 8.8 eV, followed by second unstructured and steeply rising band. Calculated VIEs and AIEs of the h-bonded and π-stacked isomers show that the low energy shoulder of the first band corresponds to the states derived from ionization of A, whereas the band maximum can be assigned to the states derived by ionization of T. The second band (rising almost linearly) covers at least seven ionized states of both AT-HB1 and AT-HB2. Overall, the broad structure of the AT derived PIE spectrum does not allow to differentiate between contributions from ionization of different isomers to the total intensity. This spectra does not show any clear evidence of the presence of π-stacked isomers.

Fig. 14 also shows the computed energy thresholds for the appearance of the protonated species, TH^+ and AH^+ (summarized in Table VI and Fig. 13). Note that different isomers of TH^+ are considered for TT-HB1, TT-HB2, and TT-HB3 dissociation, as well as different AH^+ isomers for AT-HB1 and AT-HB2 dimers. As evident from Fig. 13 and the corresponding D_0 (see Table III), the dissociation to the h-transferred fragments is energetically unfavorable relative to the dissociation to $B^{+\cdot}$ and B in TT and AA. In TT h-bonded dimers, the difference between the two channels varies from 4 to 9 kcal/mol for different isomers, however, in AA they are less 1 kcal/mol apart. In AT, the AH^++$(T–H)^{\cdot}$ channel becomes energetically favorable by about 2-3 kcal/mol relative to $A^{+\cdot}$ and T. Overall, the BH^++$(B–H)^{\cdot}$ channel appears to be very efficient in all species, as follows from the large yield of the protonated species in this study, as well as in Refs. [27, 79, 88]. This is not surprising in view of barrierless h-transfer observed in this work for TT-HB1 and by Park et al. [78] for the AA-HB1 dimer.

The experimental onsets for TH^+ and AH^+ for the pure molecular beams are 9.20 eV and 9.10 eV, respectively. The yield of TH^+ slowly rises for the photon energies between 9.20 and 9.50 eV. Above 9.5 eV there is strong increase in the yeild of TH^+, especially prominent for 9.7-9.9 eV photon energies. TH^+ onset for the mixed A and T molecular beam does not change, however, AH+ appearance energy shifts to 8.90 eV (see Supporting Information). Neglecting contributions from larger clusters, AH^+ and TH^+ can be produced from homo- and hetero-dimers. The computed thresholds can be compared to the experimental onsets assuming that the dissociation does not involve a barrier.

For the lowest energy isomer, TT-HB1, the TH^++$(T–H)^{\cdot}$ channel becomes energetically accessible at 9.91 eV, which is 0.4 eV above the sharp rise in TH^+ signal (9.5 eV). The low onset energy value can only be explained by the presence of a higher-energy isomer. The most likely candidates are π-stacked TT dimers for which these channels opens up at 9.3-9.6 eV for different TH^+ products in assumption of barrierless proton transfer (see Fig.13). Dissociation of more populated TT-HB2 and TT-HB3 dimers could explain the strong increase in the signal of TH^+ species at 9.5-9.7 eV. The most populated TT-HB1 dimer gives rise to the TH^+ signal for the photon energies above 9.9 eV. Note, however, that a possible barrier along the dissociation coordinate would result in a higher-energy onset. The threshold for the TH^+ appearance from AT-HB1 and AT-HB2 is much higher, i.e., 10.03

and 10.18 eV, respectively.

The experimentally observed onsets for AH^+ for pure (9.10 eV) and mixed beams (8.90 eV) are in relatively good agreement with 8.97 and 8.82 eV values calculated for the AA-HB1 and AT-HB1 dimers, respectively. The threshold energy for dissociation of the lowest stacked AA and AT isomers is considerably lower (8.5-8.6 eV).

Thus, both differentiated PIE and the appearance thresholds of the protonated species support the presence of more than one lowest energy h-bonded dimer and are also consistent with the presence of TT stacked dimers. However, experimental data show no evidence for the presence of stacked AA or AT isomers.

IV. CONCLUSIONS

We present a combined theoretical and experimental study of the ionized dimers of NAB thymine and adenine, TT, AA, and AT. AIEs of TT, AA and AT as well as appearance energies for AH^+ and TH^+ species are experimentally measured for the first time. The corresponding onset energies for the PIE spectra are 8.45±0.05 eV, 8.10±0.05 eV and 8.05±0.05 eV for the TT, AA and AT dimers, respectively. Appearence energies of AH^+ and TH^+ are 9.10± 0.1 and 9.20 ± 0.1 eV for pure adenine and thymine molecular beam, respectively.

Non-covalent interactions strongly affect vertical and adiabatic IEs. In TT, the largest changes in VIEs between monomer and dimer (0.4 eV) were observed in the asymmetric h-bonded and symmetric π-stacked isomers, whereas in the lowest-energy symmetric h-bonded cluster the shift is much smaller (0.1 eV). The origin of the shift and the character of the ionized states is different in asymmetric h-bonded and stacked isomers. In the former case, the initial hole is localized on one of the fragments, and the shift is due to the electrostatic stabilization of the positive charge of the ionized fragment by the dipole moment of the neutral fragment. In the latter, the hole is delocalized, and the change in IE is proportional to overlap of the fragments' MOs. The fate of the ionized states is also different: the h-bonded ones undergo barrierless (or almost barrierless) proton transfer, whereas the symmetric π-stacked ones form structures with a partially covalent bond between the fragments. For all the isomers, ionization increases the binding energy by about 10-20 kcal/mol. The onset of the PIE curve of TT dimer is at 8.45±0.05 eV, which agrees well with that of π-stacked isomers. Large geometric relaxation upon ionization (h-transfer) in the h-bonded dimers

suggests poor FCFs, whereas the shape of the experimental curve is more consistent with the π-stacked isomers for which the relaxation is less. The differentiated PIE curves show evidence of several isomers, especially in the second band derived from the ionizations from lower orbitals. The sharp rise in the signal of TH^+ at 9.50-9.70 eV agrees well with the calculated dissociation threshold energies of the asymmetric h-bonded dimers, whereas the threshold for the lowest energy h-bonded isomer is considerably higher (9.91 eV).

The AA dimer behaves differently. The shifts in IEs are much smaller due to more delocalized orbitals and less polar character of A (e.g., the dipole moment of A is almost half that of T). The latter results in less aligned π-stacked structures characterized by less efficient overlap between fragment molecular orbitals. A more delocalized orbital of A results in larger geometrical relaxation and poor FCFs for the lowest band in A and, consequently, AA. The onset of the PIE curve for AA is 8.10±0.05 eV, however, the computed AIE for the lowest isomer (h-transferred h-bonded) is much lower (7.50 eV). Additional geometric relaxation due to h-transfer is likely to be responsible for the unfavorable FCFs. The threshold for AH^+ appearance is 9.10±0.1 eV, which is in reasonable agreement with the computed threshold for the lowest energy AA isomer (symmetric h-bonded).

Measured onset on the PIE curve for the AT dimers is 8.05±0.05 eV. The analysis of VIEs reveal that the states derived from thymine ionization exhibit larger shifts that those derived from ionizations of A. Some of the AT states feature profoundly non-Koopmans character.

The pattern that emerges from our study is that the IE of T is affected more by non-covalent interactions (both stacking and h-bonding) than those of A (which has lower IE). Thus, the differences in IEs between T and A decrease due to these interactions, which might play a role facilitating efficient charge transfer through the DNA strands.

Acknowledgment

This work is conducted under auspices of the *iOpenShell* Center for Computational Studies of Electronic Structure and Spectroscopy of Open-Shell and Electronically Excited Species supported by the National Science Foundation through the CRIF:CRF CHE-0625419+0624602+0625237 grant. O.K. and M.A. acknowledge support by the Director, Office of Energy Research, Office of Basic Energy Sciences, Chemical Sciences Division of

the U.S. Department of Energy under contract No. DE-AC02-05CH11231.

Supporting Information Available

Mass spectra of the cations (10 eV), appearance energy curves for the AH^+ and TH^+ species for pure and mixed beams, EOM-IP-CCSD vertical ionization energies for A and T monomers and dimers, structures and EOM-IP-CCSD vertical ionization energies for selected cytosine dimers, NBO charges for cations of A and T dimers, optimized geometries and harmonic frequencies for A and T dimers. This material is available free of charge via the Internet at http://pubs.acs.org.

[1] Nácuteuñez, M.E. ; Hall, D.B. ; Barton, J.K. *Chem. and Biol.* **1999**, *6*, 85.

[2] Henderson, P.T. ; Jones, D. ; Hampikian, G. ; Kan, Y. ; Schuster, G.B. *Proc. Nat. Acad. Sci.* **1999**, *96*, 8353.

[3] Lewis, F.D. ; Letsinger, R.L. ; Wasielewski, M.R. *Acc. Chem. Res.* **2001**, *34*, 159.

[4] Hutchison, G.R. ; Ratner, M.A. ; Marks, T.J. *J. Am. Chem. Soc.* **2005**, *127*, 16866.

[5] Taniguchi, M. ; Kawai, T. *Physica E* **2006**, *33*, 1.

[6] Nogues, C. ; Cohen, S.R. ; Danube, S. ; Apter, N. ; Naaman, R. *J. Phys. Chem. B* **2006**, *110*, 8901.

[7] Heath, J.R. ; Ratner, M.A. *Phyisics Today* **2003**, *56*, 43.

[8] Grozema, F.C. ; Tonzani, S. ; Berlin, Y.A. ; Schatz, G.C. ; Ratner, L.D.A. Siebbeles M.A. *J. Am. Chem. Soc.* **2008**, page 5157.

[9] Goldsmith, R.H. ; DeLeon, O. ; Wilson, T.M. ; Filkenstein-Shapiro, D. ; Ratner, M.A. ; Wasilewski, M.R. *J. Phys. Chem. A* **2008**, *112*, 4410.

[10] Grozema, F.C. ; Siebbeles, L.D.A. *Int. Rev. Phys. Chem.* **2008**, *27*, 81.

[11] Shukla, M.K. ; Leszczynski, J. ; Springer, 2008; chapter Radiation inuced molecular phenomena in nucleic acids: A brief introduction, pages 1–14.

[12] Dougherty, D. ; Wittel, K. ; Meeks, J. ; McGlynn, S. P. *J. Am. Chem. Soc.* **1976**, *98*, 3815.

[13] Urano, S. ; Yang, X. ; LeBrenton, P.R. *J. Mol. Struct.* **1989**, *214*, 315.

[14] Lauer, G. ; Schäfer, W. ; Schweig, A. *Tetrahedron Lett.* **1975**, *16*, 3939.

[15] Yu, C. ; O'Donnel, T.J. ; LeBreton, P.R. *J. Phys. Chem.* **1981**, *85*, 3851.

[16] Kim, S.K. ; Lee, W. ; Herschbach, D.R. *J. Phys. Chem.* **1996**, *100*, 7933.

[17] Satzger, H. ; Townsend, D. ; Stolow, A. *Chem. Phys. Lett.* **2006**, *430*, 144.

[18] Belau, L. ; Wilson, K.R. ; Leone, S.R. ; Ahmed, M. *J. Phys. Chem. A* **2007**, *111*, 7562.

[19] Cauët, E. ; Dehareng, D. ; Liévin, J. *J. Phys. Chem. A* **2006**, *110*, 9200.

[20] Roca-Sanjuán, D. ; Rubio, M. ; Merchán, M. ; Serrano-Andrés, L. *J. Chem. Phys.* **2006**, *125*, 084302.

[21] Cauët, E. ; Liévin, J. *Adv. Quantum Chem.* **2007**, *52*, 121.

[22] Hudock, H.R. ; Levine, B.G. ; Thompson, A.L. ; Satzger, H. ; Townsend, D. ; Gador, N. ; Ulrich, S. ; Stolow, A. ; Martínez, T.J. *J. Phys. Chem. A* **2007**, *111*, 8500.

[23] Crespo-Hernández, C.E. ; Cohen, B. ; Hare, P.M. ; Kohler, B. *Chem. Rev.* **2004**, *104*, 1977.

[24] He, Y. ; Wu, C. ; Kong, W. *J. Phys. Chem. A* **2004**, *108*, 943.

[25] Yoshikawa, A. ; Matsika, S. *Chem. Phys.* **2008**, *347*, 393.

[26] Crespo-Hernández, C.E. ; Kohen, B. ; Kohler, B. *Nature* **2005**, *436*, 1141.

[27] Gador, N. ; Samoylova, E. ; Smith, V.R. ; Stolow, A. ; Rayner, D.M. ; Radloff, W. ; Hertel, I.V. ; Schultz, T. *J. Phys. Chem. A* **2007**, *111*, 11743.

[28] Lange, A.W. ; Herbert, J.M. *J. Am. Chem. Soc.* **2009**, *131*, 3913.

[29] Fernando, H. ; Papadantonakis, G.A. ; Kim, N.S. ; LeBreton, P.R. *Proc. Nat. Acad. Sci.* **1998**, *95*, 5550.

[30] Slavíček, P. ; Winter, B. ; Faubel, M. ; Bradforth, S.E. ; Jungwirth, P. *J. Am. Chem. Soc.* **2009**, *131*, 6460.

[31] Crespo-Hernández, C. ; Close, D.M. ; Gorb, L. ; Leszczynski, J. *J. Phys. Chem. B* **2007**, *111*, 5386.

[32] Golubeva, A.A. ; Krylov, A.I. *Phys. Chem. Chem. Phys.* **2009**, *11*, 1303.

[33] Sugiyama, H. ; Saito, I. *J. Am. Chem. Soc.* **1996**, *118*, 7063.

[34] Prat, F. ; Houk, K.N. ; Foote, C.S. *J. Am. Chem. Soc.* **1998**, *120*, 845.

[35] Schumm, S. ; Prévost, M. ; Garcia-Fresnadillo, D. ; Lentzen, O. ; Moucheron, C. ; Krisch-De Mesmaeker, A. *J. Phys. Chem. B* **2002**, *106*, 2763.

[36] Colson, A.-O. ; Besler, B. ; Sevilla, M.D. *J. Phys. Chem.* **1992**, *96*, 9787.

[37] Colson, A.-O. ; Besler, B. ; Sevilla, M.D. *J. Phys. Chem.* **1993**, *97*, 13852.

[38] Roca-Sanjuán, D. ; Merchán, M. ; Serrano-Andrés, L. *Chem. Phys.* **2008**, *349*, 188.

[39] Berkowitz, J. *J. Chem. Phys.* **1978**, *69*, 3044.

[40] Hobza, P. ; Špone, J. ; Reschel, T. *J. Comput. Chem.* **1995**, *16*, 1315.

[41] Dabkowska, I. ; Jurečka, P. ; Hobza, P. *J. Chem. Phys.* **2005**, *122*, 204322.

[42] Grimme, S. *J. Comput. Chem.* **2004**, *25*, 1463.

[43] Grimme, S. *J. Comput. Chem.* **2006**, *27*, 1787.

[44] Jurečka, P. ; Hobza, P. *J. Am. Chem. Soc.* **2003**, *125*, 15608.

[45] Chai, J.-D. ; Head-Gordon, M. *Phys. Chem. Chem. Phys.* **2008**, *10*, 6615.

[46] Lebedev, V.I. *Zh. Vychisl. Mat. Mat. Fiz.* **1975**, *15*, 48.

[47] Murray, W.C. ; Handy, N.C. ; Laming, G.J. *Mol. Phys.* **1993**, *78*, 997.

[48] Bartlett, R.J. *Int. J. Mol. Sci.* **2002**, *3*, 579.

[49] Stanton, J.F. ; Gauss, J. *Adv. Chem. Phys.* **2003**, *125*, 101.

[50] Krylov, A.I. *Annu. Rev. Phys. Chem.* **2008**, *59*, 433.

[51] Pal, S. ; Rittby, M. ; Bartlett, R.J. ; Sinha, D. ; Mukherjee, D. *Chem. Phys. Lett.* **1987**, *137*, 273.

[52] Stanton, J.F. ; Gauss, J. *J. Chem. Phys.* **1994**, *101*, 8938.

[53] Kamyia, M. ; Hirata, S. *J. Chem. Phys.* **2006**, *125*, 074111.

[54] Pieniazek, P.A. ; Arnstein, S.A. ; Bradforth, S.E. ; Krylov, A.I. ; Sherrill, C.D. *J. Chem. Phys.* **2007**, *127*, 164110.

[55] Pieniazek, P.A. ; Bradforth, S.E. ; Krylov, A.I. *J. Chem. Phys.* **2008**, *129*, 074104.

[56] Pieniazek, P.A. ; Krylov, A.I. ; Bradforth, S.E. *J. Chem. Phys.* **2007**, *127*, 044317.

[57] Pieniazek, P.A. ; VandeVondele, J. ; Jungwirth, P. ; Krylov, A.I. ; Bradforth, S.E. *J. Phys. Chem. A* **2008**, *112*, 6159.

[58] Pieniazek, P.A. ; Sundstrom, E.J. ; Bradforth, S.E. ; Krylov, A.I. *J. Phys. Chem. A* **2009**, *113*, 4423.

[59] Landau, A. ; Krylov, A.I. *J. Chem. Phys.* **2009;** submitted.

[60] Weinhold, F. ; Landis, C. R. *Chem. Ed.: Res. & Pract. Eur.* **2001**, *2*, 91.

[61] Golubeva, A.A. ; Pieniazek, P.A. ; Krylov, A.I. *J. Chem. Phys.* **2009**, *130*, 124113.

[62] Y. Shao, L.F. Molnar, Y. Jung, J. Kussmann, C. Ochsenfeld, S. Brown, A.T.B. Gilbert, L.V. Slipchenko, S.V. Levchenko, D.P. O'Neil, R.A. Distasio Jr, R.C. Lochan, T. Wang, G.J.O. Beran, N.A. Besley, J.M. Herbert, C.Y. Lin, T. Van Voorhis, S.H. Chien, A. Sodt, R.P. Steele, V.A. Rassolov, P. Maslen, P.P. Korambath, R.D. Adamson, B. Austin, J. Baker, E.F.C. Bird, H. Daschel, R.J. Doerksen, A. Drew, B.D. Dunietz, A.D. Dutoi, T.R. Furlani, S.R. Gwaltney, A. Heyden, S. Hirata, C.-P. Hsu, G.S. Kedziora, R.Z. Khalliulin, P. Klunziger, A.M. Lee, W.Z. Liang, I. Lotan, N. Nair, B. Peters, E.I. Proynov, P.A. Pieniazek, Y.M. Rhee, J. Ritchie, E. Rosta, C.D. Sherrill, A.C. Simmonett, J.E. Subotnik, H.L. Woodcock III, W. Zhang, A.T. Bell, A.K. Chakraborty, D.M. Chipman, F.J. Keil, A. Warshel, W.J. Herhe, H.F. Schaefer III, J. Kong, A.I. Krylov, P.M.W. Gill, M. Head-Gordon *Phys. Chem. Chem. Phys.* **2006**, *8*, 3172.

[63] Müller-Dethlefs, K. ; Hobza, P. *Chem. Rev.* **2000**, *100*, 143.

[64] Sponer, J. ; Leszczynski, J. ; Hobza, P. *Biopolimers* **2002**, *61*, 3.

[65] Saigusa, H. *Photochem. Photobiol.* **2006**, *7*, 197.

[66] de Vries, M.S. ; Hobza, P. *Annu. Rev. Phys. Chem.* **2007**, *58*, 585.

[67] Kabeláč, M. ; Hobza, P. *Chem. Eur. J.* **2001**, *7*, 2067.

[68] Kabelač, M. ; Hobza, P. *J. Phys. Chem. B* **2001**, *105*, 5804.

[69] Ran, J. ; Hobza, P. *J. Phys. Chem. B* **2009**, *113*, 2933.

[70] Plützer, C. ; Hünig, I. ; Kleinermanns, K. ; Nir, E. ; de Vries, M.S. *ChemPhysChem* **2003**, *4*, 838.

[71] Kratochvil, M. ; Engkvist, O. ; Sponer, J. ; Jungwirth, P. ; Hobza, P. *J. Phys. Chem. A* **1998**, *102*, 6921.

[72] de Vries, M.S. ; Springer, 2008; chapter Isolated DNA base pairs, interplay between theory and experiment, pages 323–341.

[73] Plützer, Chr. ; Nir, E. ; de Vries, M.S. ; Kleinermanns, K. *Phys. Chem. Chem. Phys.* **2001**, *3*, 5466.

[74] Oana, C.M. ; Krylov, A.I. *J. Chem. Phys.* **2007**, *127*, 234106.

[75] Stoll, H. ; Wagenblast, G. ; Preuß, H. *Theor. Chim. Acta* **1980**, *57*, 169.

[76] Valeev, E.F. ; Coropceanu, V. ; da Silva Filho, D.A. ; Salman, S. ; Brédas, J.-L. *J. Am. Chem. Soc.* **2006**, *128*, 9882.

[77] Bravaya, K. B. ; Kostko, O. ; Ahmed, M. ; Dolgikh, S. ; Landau, A. ; Krylov, A.I. **2009;** in preparation.

[78] Park, H.S. ; Nam, S.H. ; Song, J.K. ; Park, S.M. ; Ryu, S. *J. Phys. Chem. A* **2008**, *112*, 9023.

[79] Nam, S.H. ; Park, H.S. ; Ryu, S. ; Song, J.K. ; Park, S.M. *Chem. Phys. Lett.* **2008**, *450*, 236.

[80] Candeias, L.P. ; Steenken, S. *J. Am. Chem. Soc.* **1989**, *111*, 1094.

[81] Steenken, S. *Chem. Rev.* **1989**, *89*, 503.

[82] Hutter, M. ; Clark, T. *J. Am. Chem. Soc.* **1996**, *118*.

[83] Ghosh, A.K. ; Schuster, G.B. *J. Am. Chem. Soc.* **2006**, *128*, 4172.

[84] Kumar, A. ; Sevilla, M.D. *J. Phys. Chem. B* **2009;** asap.

[85] Bertrani, J. ; Oliva, A. ; Rodríguez-Santiago, L. ; Sodupe, M. *J. Am. Chem. Soc.* **1998**, *120*, 8159.

[86] Sobolewski, A.L. ; Domcke, W. ; Hättig, C. *Proc. Nat. Acad. Sci.* **2005**, *102*, 17903.

[87] Perun, S. ; Sobolewski, A.L. ; Domcke, W. *J. Phys. Chem. A* **2006**, *110*, 9031.

[88] Hünig, I. ; Plützer, C. ; Seefeld, K.A. ; Löwenich, D. ; Nispel, M. ; Kleinermanns, K. *Comp. Phys. Comm.* **2004**, *5*, 1427.